23rd International Conference on Renewable Energies and Power Quality (ICREPQ'25)
Tenerife (Spain), 25th to 27th June 20245
Renewable Energy and Power Quality Journal (RE&PQJ)
ISSN 2172-038 X, Volume No.23, September 2025

A study on the negative sequence current injection during LVRT of IBRs

A. Blázquez[1], M. Larruskain[1], E. Torres[1], P. Eguia[1], A. Castañon[2] and R. Cimadevilla[2]

[1] Department of Electrical Engineering
ESI-Bilbao, University of the Basque Country (UPV/EHU)
Plaza Ingeniero Torres Quevedo 1, 48013 Bilbao (Spain)

[2] ZIV
Parque Tecnológico 210, 48100 Zamudio (Spain)

Abstract. Low Voltage Ride Through (LVRT) behaviour of Inverter Based Resources (IBR) during asymmetrical grid faults is dictated by the requirements of Grid Code (GC) at the Point of Common Coupling (PCC) of the renewable energy plants. Earlier GCs demanded only positive sequence current injection, which gave freedom to inverter manufacturers to implement different negative sequence injection strategies, while newer GCs define specific negative sequence current injection requirements. The existence of different negative sequence current control strategies during grid faults creates problems for line protection relays, as fault detection algorithms malfunction for certain angle relationships between the negative sequence voltage and current phasors.
This paper analyses different negative sequence injection algorithms of IBRs and demonstrates certain relationships between sequence impedances of the inverter that can be used for improving line protection algorithms. The analytical findings are confirmed via Real Time simulations of a Type 4 wind farm connected to a power system with different network strength characteristics.

Key words. IBR, Grid Code, LVRT, Negative Sequence, Line Protection.

1. Introduction

The connection of new renewable energy generators to the electric energy system has an effect on network protection [1], [2]. Most of the new generators use power electronic converters to interface with the grid, either partial power converters or full power converters, and are known, in general, as Inverter Based Resources (IBR). IBRs response during system faults is different from the response of traditional synchronous generators. On the one hand, the magnitude of the current is limited around the nominal value and, on the other hand, its characteristics in terms of sequence components are governed by the control algorithms used during Low Voltage Ride Though (LVRT) operation. LVRT operation of IBRs is dictated by the Grid Code (GC) requirements, which, in turn, influence how the different IBR manufacturers implement their LVRT controls and, in the end, the behaviour of the renewable energy plants during short circuits in the grid.

Initially, and still in use in different countries, GCs required only positive sequence reactive current injection. This gave freedom to the IBR manufacturers to implement different negative sequence control strategies during asymmetrical faults. Modern GCs, like the German or Spanish ones [3]-[4], specify in more detail the expected response of the IBR in terms of positive and negative sequence current injection.

Consequently, there is a large fleet of renewable generation plants connected to power systems with different behaviour under similar asymmetrical fault conditions, which, in turn produce mal and misoperations of protection relays [5]. [6]-[8] have studied the effect of the different types of IBRs on different types of line protection relays, like distance, directional current or differential. As a result, new or modifications to actual protection algorithms have been proposed [5], [9]. However, these solutions are valid for the specific negative sequence control of the IBR used in the modeling of the fault response.

This paper analyses the response of full converter IBRs to asymmetrical faults according to different negative sequence control algorithms. The objective is to characterize this response so protection algorithms can be designed that are valid for any renewable power plant interfaced with an inverter. This will improve the reliability of modern power systems.

The paper is structured in five sections, including this introduction. Section 2 details the different negative sequence control algorithms for LVRT considered and studies analytical expressions for the impedance of the converter during asymmetrical faults. Section 3 details the simulation study case used to prove the analysis in Section 2. Section 4 shows some examples for different asymmetrical faults and Section 5 concludes the paper.

2. Negative sequence current controls during LVRT

The converter current control uses a decoupled double synchronous reference frame for the conversion and independent control of inverter positive and negative sequence currents. Under normal operating conditions, only positive sequence current is delivered, but when a fault condition is detected, the converter also provides negative sequence current. In this paper, three different strategies have been considered for negative sequence current control: two power oscillations suppression controls and a control adapted to the Spanish GC.

A. Power oscillations suppression controls

Under unbalanced conditions, the interaction of voltage and current components with different sequences produces double frequency oscillations in both instantaneous active and reactive powers. Equation (1) expresses the average active (P) and reactive (Q) powers and the active (P_c, P_s) and reactive (Q_c, Q_s) power oscillating terms as a function of positive and negative dq components of voltage and current measured at the point of common coupling (PCC), in two synchronous reference frames rotating at the fundamental grid frequency ω and -ω.

$$\begin{bmatrix} \boldsymbol{P} \\ \boldsymbol{Q} \\ \boldsymbol{P_c} \\ \boldsymbol{P_s} \\ \boldsymbol{Q_c} \\ \boldsymbol{Q_s} \end{bmatrix} = \begin{bmatrix} \boldsymbol{v_d^+} & \boldsymbol{v_q^+} & \boldsymbol{v_d^-} & \boldsymbol{v_q^-} \\ \boldsymbol{v_q^+} & \boldsymbol{-v_d^+} & \boldsymbol{v_q^-} & \boldsymbol{-v_d^-} \\ \boldsymbol{v_d^-} & \boldsymbol{v_q^-} & \boldsymbol{v_d^+} & \boldsymbol{v_q^+} \\ \boldsymbol{v_q^-} & \boldsymbol{-v_d^-} & \boldsymbol{-v_q^+} & \boldsymbol{v_d^+} \\ \boldsymbol{v_q^-} & \boldsymbol{-v_d^-} & \boldsymbol{v_q^+} & \boldsymbol{-v_d^+} \\ \boldsymbol{-v_d^-} & \boldsymbol{-v_q^-} & \boldsymbol{v_d^+} & \boldsymbol{v_q^+} \end{bmatrix} \times \begin{bmatrix} \boldsymbol{i_d^+} \\ \boldsymbol{i_q^+} \\ \boldsymbol{i_d^-} \\ \boldsymbol{i_q^-} \end{bmatrix} \quad (1)$$

From the inversion of (1), positive and negative dq reference currents to provide reference power with ripple control can be obtained. In three-wire converter systems there are only four controllable magnitudes (i_d^+, i_q^+, i_d^-, i_q^-), so only four control targets can be selected and different negative sequence current control strategies can be adopted: constant instantaneous active power control, reactive power control and balanced current control [10].

Negative sequence reference currents required for power ripple elimination can be calculated as a function of the positive sequence reference currents required for a reference active and reactive power, using (2) and (3) [7]:

$$\boldsymbol{I_{d,ref}^-} = \boldsymbol{K}\left(\frac{v_d^+ v_d^- - v_q^+ v_q^-}{(v_d^+)^2+(v_q^+)^2}\right)\boldsymbol{I_{d,ref}^+} + \boldsymbol{K}\left(\frac{v_d^+ v_q^- + v_d^- v_q^+}{(v_d^+)^2+(v_q^+)^2}\right)\boldsymbol{I_{q,ref}^+} \quad (2)$$

$$\boldsymbol{I_{q,ref}^-} = \boldsymbol{K}\left(\frac{v_d^+ v_q^- + v_d^- v_q^+}{(v_d^+)^2+(v_q^+)^2}\right)\boldsymbol{I_{d,ref}^+} + \boldsymbol{K}\left(\frac{v_d^+ v_q^- - v_d^+ v_d^-}{(v_d^+)^2+(v_q^+)^2}\right)\boldsymbol{I_{q,ref}^+} \quad (3)$$

where K must be equal to +1 for constant reactive power control or equal to -1 for constant active power control. In addition, current limitation can be carried out by means of a scaling factor (SF) calculated using (4) to scale down the positive and negative reference currents in case they result in converter exceeding its current limit (I_{max}).

$$\boldsymbol{SF} = \frac{\sqrt{\left(i_{d,ref}^+\right)^2+\left(i_{q,ref}^+\right)^2}+\sqrt{\left(i_{d,ref}^-\right)^2+\left(i_{q,ref}^-\right)^2}}{\boldsymbol{I_{max}}} \quad (4)$$

B. Spanish grid code control

In the case of unbalanced faults, the Spanish grid code [3] requires converters to inject/absorb negative sequence current (ΔI_2) as a function of the change in the negative sequence voltage (ΔV_2), according to a proportional control with gain K_2, to emulate the natural behaviour of a synchronous generator (5):

$$\Delta \boldsymbol{I_2} = \boldsymbol{K_2} \cdot \Delta \boldsymbol{V_2} \quad (5)$$

As a result, only reactive negative sequence current is required during faults, with a phase difference of 90º with negative sequence voltage. In addition, the grid code establishes reactive current priority during faults and injection of active current only for the rest up to maximum current.

C. Inverter impedances during LVRT

Positive and negative impedances of the converter, as seen from the PCC, can be calculated as the quotient of voltage and current phasors of the corresponding sequence.

In the case of the Spanish grid code, the negative sequence impedance is purely reactive, as only reactive negative sequence current is provided. In the case of power oscillation suppression control, the behaviour of the negative sequence impedance can be obtained from the simplification of equations (2) and (3), assuming that "d" axis of dq reference frames for positive and negative sequence control are synchronized with positive and negative sequence voltage phasors:

$$\boldsymbol{I_{d,ref}^-} = \boldsymbol{K}\,\frac{\boldsymbol{v_d^-}}{\boldsymbol{v_d^+}}\,\boldsymbol{I_{d,ref}^+} \quad (6)$$

$$\boldsymbol{I_{q,ref}^-} = \boldsymbol{-K}\,\frac{\boldsymbol{v_d^-}}{\boldsymbol{v_d^+}}\,\boldsymbol{I_{q,ref}^+} \quad (7)$$

Then, the negative sequence current and the negative sequence impedance of the converter are given by:

$$\underline{\boldsymbol{I_2}} = \boldsymbol{I_d^-} + \boldsymbol{j I_q^-} = \boldsymbol{K}\,\frac{\boldsymbol{v_d^-}}{\boldsymbol{v_d^+}}\left(\boldsymbol{I_d^+} - \boldsymbol{j}\,\boldsymbol{I_q^+}\right) = \boldsymbol{K}\,\frac{\boldsymbol{v_d^-}}{\boldsymbol{v_d^+}}\,\underline{\boldsymbol{I_1}}^* \quad (8)$$

$$\underline{\boldsymbol{Z_2}} = \frac{\underline{\boldsymbol{V_2}}}{\underline{\boldsymbol{I_2}}} = \frac{\boldsymbol{v_d^+}}{\boldsymbol{K}(\boldsymbol{I_d^+} - \boldsymbol{j}\,\boldsymbol{I_q^+})} = \frac{\underline{\boldsymbol{V_1}}}{\boldsymbol{K}\cdot\underline{\boldsymbol{I_1}}^*} \quad (9)$$

It can be observed that positive and negative sequence impedances have the same magnitude under constant active power control ($K = -1$) and reactive power control ($K = +1$). However, their angles depend on the control strategy as, whereas the relative angle between positive and negative voltage and current are similar under constant reactive power control ($K = +1$), a phase difference of 180º appears in the case of constant active power control ($K = -1$).

3. Study case

To validate the proposed negative sequence injection methods, various simulations have been carried out in OPAL-RT real time simulator of a type 4 wind farm connected to an AC grid, developed from [11].

A. Network model

Figure 1 illustrates the implemented electrical network model, which represents the integration of a Type 4 wind farm into a power system. The grid is represented by a 120 kV AC voltage source with variable short circuit strength to simulate a variable short-circuit ratio (SCR), being 100 MVA for SCR = 9 and 30 MVA for SCR = 2.7.

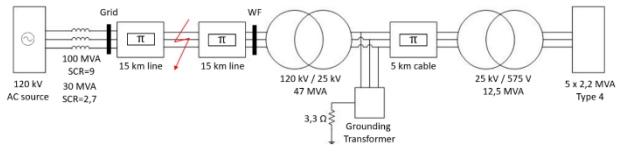

Fig.1. Network model in Matlab/Simulink

Tables I and II show the configuration parameters for the AC source and the equivalent grid impedance.

Table I. – AC grid parameters

AC Three-Phase Source	U_{AC}	120 kV
	f	60 Hz

Table II. – AC grid impedance

AC impedance	R_1	0,1 Ω
	L_1	1 H
	R_0	0,3 Ω
	L_0	3 H
	S	100 MVA

The plant is connected through a 30 km overhead transmission line and a 120 kV/25 kV power transformer rated at 47 MVA. The line is divided into two sections to simulate line faults. Table III shows the configuration parameters of the transmission line and Table IV the parameters of the HV-MV power transformer.

Table III. – Line parameters

30 km line	R_1	0,176 Ω/km
	L_1	1,57e-3 H/km
	C_1	0,0127e-6 F/km
	R_0	0,42 Ω/km
	L_0	3,82e-3 H/km
	C_0	0,007e-6 F/km

Table IV. – HV-MV transformer parameters

HV-MV transformer	V_1	120 kV
	V_2	25 kV
	S	47 MVA
	Ucc	16%

The wind farm´s internal network is modelled with an equivalent 5 km underground cable, shown in Table V, and an equivalent 25 kV/575 V turbine transformer with a capacity of 12.5 MVA, as shown in Table VI. The MV network is grounded using a grounding transformer with a resistance of 3.3 Ω.

Table V. – MV cable parameters

5 km cable	R_1	0,1153 Ω/km
	L_1	1,05e-3 H/km
	C_1	11,33e-9 F/km
	R_0	0,413 Ω/km
	L_0	3,32e-3 H/km
	C_0	5,01e-9 F/km

Table VI. – MV-LV transformer parameters

MV-LV transformer	V_1	25 kV
	V_2	575 V
	S	12,5 MVA
	Ucc	5 %

Finally, the 5 wind turbines are modelled with an equivalent Type 4 wind turbine generator (WTG) rated to 5 times 2.2 MVA, as in Table VII. Type 4 wind turbines operate with a full-scale power converter, consisting of a back-to-back voltage source converter (VSC) topology. This configuration includes a machine-side converter (MSC) and a grid-side converter (GSC), which completely decouple the generator from the grid frequency. The full converter system enables independent control of active and reactive power, providing enhanced grid support capabilities such as voltage regulation, frequency control, and fault ride-through (FRT) capability. This topology allows the use of variable-speed wind turbines, in this case it is equipped with permanent magnet synchronous generators (PMSGs) operating in full converter mode.

This wind farm configuration ensures high efficiency, improved power quality, and better grid compliance compared to other wind turbine technologies. The fully rated power converter also allows for precise grid integration, mitigating voltage fluctuations and enhancing the overall stability of the electrical network.

Table VII. – Wind turbine parameters

Type 4 WTG	P_{rated}	5*2 MW
	S_{rated}	5*2.2 MVA
	U_{dc}	1100 V

B. Fault cases

A total of 288 fault cases have been simulated at the middle of the export transmission line, corresponding to the variation of the parameters shown in Table VIII. In all cases the wind farm is producing its rated active power.

Table VIII. – Fault parameters

Source Strenght	SCR	9; 2.7
Fault type	Fault	ABC, AB, ABG, AG
Fault resistance	Rf	0.01; 5; 50 Ohm
Pre Fault Q	Q	0; 0.33pu; -0.33pu
I2 control type	4	0; Const P; Const Q; Spanish GC

4. LVRT behaviour during asymmetrical grid faults

To highlight the different behaviour of the IBR during asymmetrical faults, this section shows the response of the different negative sequence control algorithms to different asymmetrical faults.

A. Phase to phase fault behaviour

Fig. 2 to 4 show the three phase voltage at the inverter terminals and the three phase currents injected by the inverter for the three different negative sequence control algorithms, constant P, constant Q and the Spanish grid code. The fault studied is an AB fault at the middle of the line with no fault resistance and for the case where the windfarm is operating at unity power factor and the SCR is 9.

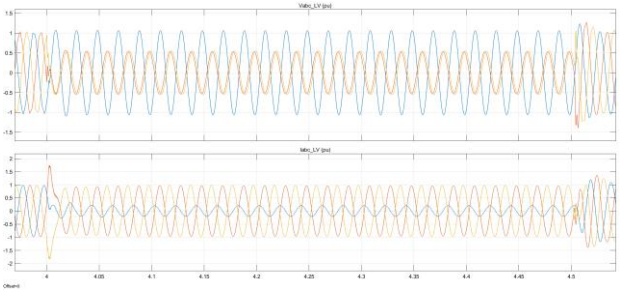

Fig.2. Phase voltages and currents. AB fault. Const P control

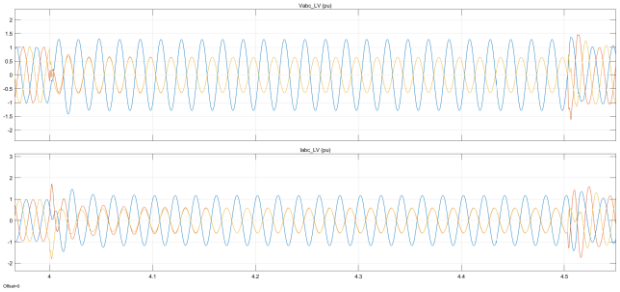

Fig.3. Phase voltages and currents. AB fault. Const Q control

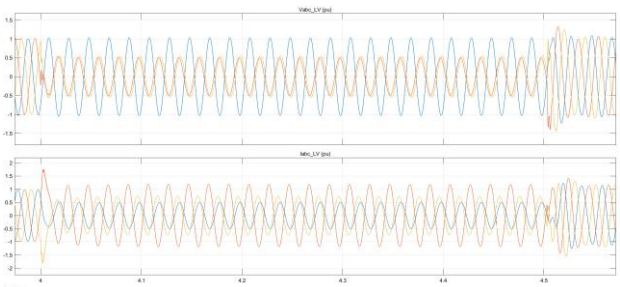

Fig.4. Phase voltages and currents. AB fault. Spanish grid code control

A visual inspection of the waveforms clearly indicates that, while the three phase voltages are the same, the three phase currents differ for each negative sequence current control during LVRT. The calculation of the positive and negative voltage, current and impedance phasors, after the initial fault transient dies out gives the results shown in Table IX, in pu of the nominal values of the inverter.

Table IX. – V, I and Z sequence phasors in p.u. AB fault

	Const P control		Const Q control		Spanish Grid Code control	
	Mod	Ang	Mod	Ang	Mod	Ang
V_1	0,598	-59,6	0,645	-57,7	0,581	-52,3
I_1	0,636	47,9	0,583	52,4	0,702	80,8
V_2	0,465	-60,9	0,646	-57,7	0,451	-55,4
I_2	0,453	-130,4	0,595	51,9	0,490	-145,3
Z_1	0,941	-107,5	1,105	-110,1	0,828	-133,1
Z_2	1,025	69,5	1,086	-109,6	0,921	89,9

B. Phase to phase to ground fault behaviour

Fig. 5 to 7 show the three phase voltages and currents at the inverter terminals for the three different negative sequence control algorithms. The fault studied is an ABG fault at the middle of the line with no fault resistance and for the case where the windfarm is operating at unity power factor and the SCR is 9.

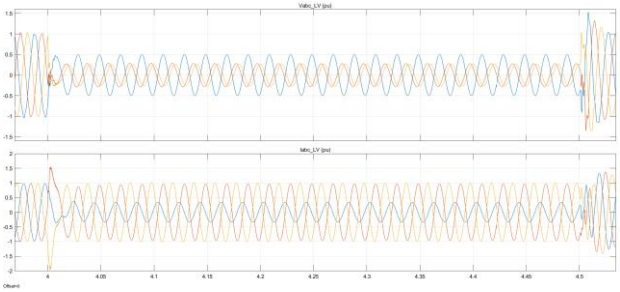

Fig.5. Phase voltages and currents. ABG fault. Const P control

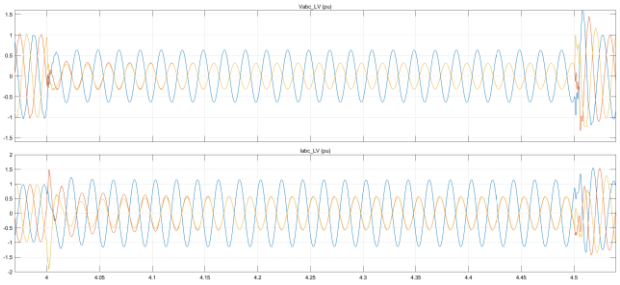

Fig.6. Phase voltages and currents. ABG fault. Const Q control

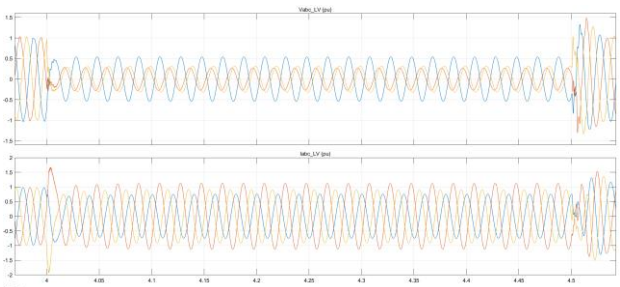

Fig.7. Phase voltages and currents. ABG fault. Spanish grid code control

For the phase to phase to ground fault, the behavior is similar. The current injection is different for the three different negative sequence current controls during LVRT. Table X shows the corresponding positive and negative voltage, current and impedance phasors, after the initial fault transient dies out.

Table X. – V, I and Z sequence phasors in p.u. ABG fault

	Const P control		Const Q control		Spanish Grid Code control	
	Mod	Ang	Mod	Ang	Mod	Ang
V_1	0,315	-61,6	0,316	-60,7	0,336	-48,5
I_1	0,722	39,1	0,562	40,2	0,917	73,0
V_2	0,181	-60,0	0,318	-57,7	0,207	-55,4
I_2	0,390	-138,3	0,577	51,9	0,220	-145,3
Z_1	0,436	-100,6	0,562	-100,9	0,366	-121,5
Z_2	0,464	78,4	0,551	-100,6	0,941	89,9

C. Phase to ground fault behaviour

Fig. 8 to 10 show the three phase voltages and currents at the inverter terminals for the three different negative sequence control algorithms. The fault studied is an AG fault at the middle of the line with no fault resistance and for the case where the windfarm is operating at unity power factor and the SCR is 9.

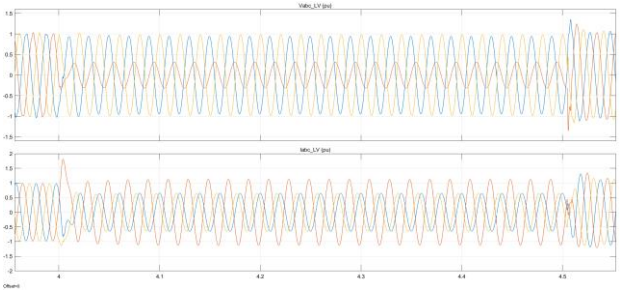

Fig.8. Phase voltages and currents. AG fault. Const P control

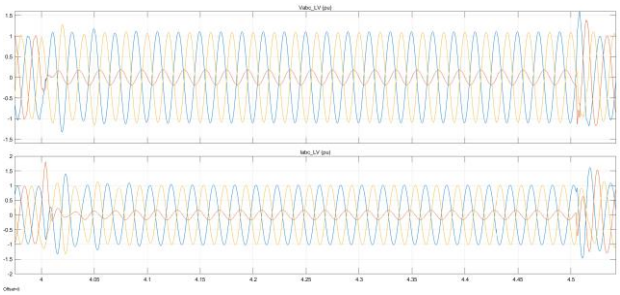

Fig.9. Phase voltages and currents. AG fault. Const Q control

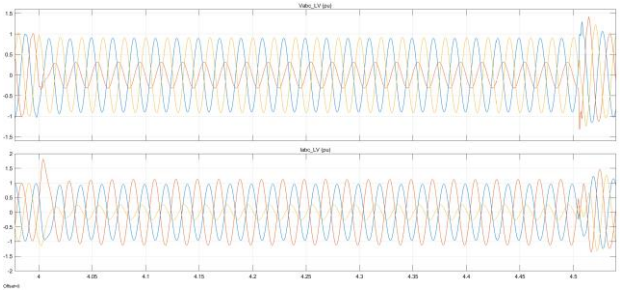

Fig.10. Phase voltages and currents. AG fault. Spanish grid code control

For the phase to ground fault, the behavior is similar, the current injection depends on the negative sequence current control mode during LVRT. Table XI shows the corresponding positive and negative voltage, current and impedance phasors, after the initial fault transient dies out.

Table XI. – V, I and Z sequence phasors in p.u. AG fault

	Const P control		Const Q control		Spanish Grid Code control	
	Mod	Ang	Mod	Ang	Mod	Ang
V_1	0,706	-57,2	0,724	-54,6	0,672	-53,2
I_1	0,748	60,0	0,664	68,9	0,704	79,7
V_2	0,394	-121,6	0,542	-113,7	0,359	-115,0
I_2	0,373	-179,8	0,504	9,1	0,501	155,1
Z_1	0,944	-117,2	1,090	-123,5	0,955	-132,9
Z_2	1,056	58,2	1,075	-122,8	0,717	-270,1

D. Comparison

For the three different unbalanced faults studied, the results collected in Tables IX to XI are in accordance with the analysis done in section 3. When the inverter controls the negative sequence current to cancel active power oscillations, the positive and negative impedance at the inverter terminals are the same, but 180º out of phase. If the inverter controls the negative sequence current injection to cancel the reactive power oscillations, the positive and negative sequence impedances are the same, in magnitude and angle. Finally, when the inverter controls the negative sequence current injection according to the Spanish grid code, this injection is done with 90º displacement from the negative sequence voltage.

We can analyze the angle relationship between the negative sequence voltage and current by plotting the results in a phasor diagram, like the one shown in Figure 11 for the three unbalanced fault cases analyzed.

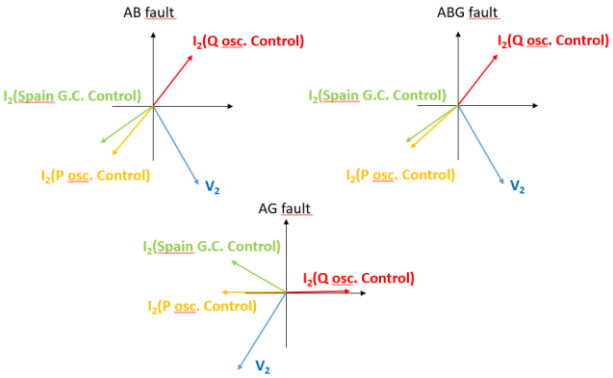

Fig.11. Comparison of I2 current injection for the three different controls.

The injection according to the Spanish grid code control mimics the behaviour of a synchronous generator, the negative sequence current lags the negative sequence voltage by 90º. The control that injects negative sequence current to cancel active power oscillations during the fault produces a similar behaviour although with a lower lagging angle. However, the injection of negative sequence current to cancel reactive power oscillations during the fault behaves in the opposite way, the negative sequence current leads the negative sequence voltage by

an angle larger than 90º. This control causes maloperation of protection relays that base their operation in negative sequence relationships, as discussed in [12].

5. Conclusion

IBR behaviour during asymmetrical faults depends on the type of negative sequence current control implemented in the inverter, which, in turn, depends on the LVRT requirements imposed by the grid code of the corresponding network to which the IBR is connected. This affects the operation of protection relays, which can experience underreach and overreach misoperations, depending on the type of control implemented. This paper has demonstrated that it is possible to obtain an analytical relationship between the positive and negative impedances at the inverter terminals. The analysis of the angles between positive and negative sequence voltages and currents by a protection relays can allow detecting the different types of negative sequence control and, enable operation accordingly to avoid misoperation of the relay.

Acknowledgement

This work has been funded by the Basque Government via RESINET project grant (KK-2023/00042) and GISEL Research Group grant (IT1522-22).

References

[1] M. Bini, et al., Challenges and solutions in the protection of transmission lines connecting nonconventional power sources, 48th Annual Western Protective Relay Conference, 2021

[2] D. Martin, P. Sharma, A. Sinclair and D. Finney, "Distance protection in distribution systems: How it assists with integrating distributed resources," 2012 65th Annual Conference for Protective Relay Engineers, College Station, TX, USA, 2012, pp. 166-177.

[3] Orden TED/749/2020, de 16 de julio, por la que se establecen los requisitos técnicos para la conexión a la red necesarios para la implementación de los códigos de red de conexión, 2020.

[4] Technical Connection Rules for High-Voltage (VDE-AR-N 4120)

[5] Felipe V. Lopes; Moisés J. B. B. Davi; Mário Oleskovicz; Ali Hooshyar; Xinzhou Dong; Adonias A. A. Neto, “Maturity Analysis of Protection Solutions for Power Systems Near Inverter-Based Resources”, IEEE Transactions on Power Delivery, Vol. 39, No. 5, October 2024

[6] A. Castañon, R. Cimadevilla, P. Eguia, E. Torres and R. Ibarra, "Impact of Wind Generation on Line Protection," PAC World Conference 2021, On Line, 2021.

[7] Liu, D., Hong, Q., Dysko, A., Tzelepis, D., Yang, G., Booth, C., Cowan, I., Ponnalagan, B.: 'Evaluation of HVDC system`s impact and quantification of synchronous compensation for distance protection', IET Renewable Power Generation, 2022, 16, (9), pp.1925-1940.

[8] Kasztenny B., “Distance elements for line protection applications near unconventional sources,” in Proc. 58th Annu. Minnesota Power Syst. Conf., 2022, pp. 1–18.

[9] R. Cimadevilla, A. Castañon, “Advanced Phase Selector for Severe Line Protection Requirements”, PAC World Conference 2022, Prague

[10] Kabiri R., Grahame D., McGrath B.P., “Control of active and reactive power ripple to mitigate unbalanced grid voltages”, IEEE Transactions on Industry Applications, Vol. 52, No. 2, pp. 1660-1668, March/April 2016.

[11] R. Gagnon, J. Brochu, “Wind Farm - Synchronous Generator and Full Scale Converter (Type 4) Average Model”, Specialized Power System Documentation, Matlab/Simulink R2017b.

[12] R. Cimadevilla, A. Castañon, P. Eguia, E. Torres, A. Blázquez, “Abnormal fault patterns in the presence of invertir based generation and their effect on line protection”, DPSP Europe 2025, 1-3 April 2025, Bilbao (Spain).